Progress In Electromagnetics Research, PIER 70, 225–246, 2007

EFFECT OF INTERNAL RESONANCE ON THE RADAR CROSS SECTION AND SHIELD EFFECTIVENESS OF OPEN SPHERICAL ENCLOSURES

K. F. A. Hussein

Microwave Engineering Department
Electronics Research Institute
Dokki, Cairo, Egypt

Abstract—In this paper, the effects of the internal resonances of an open conducting spherical enclosure with circular aperture on its radar cross section (RCS) and shield effectiveness (SE) are studied over a wide frequency band. The sizes of the spherical enclosures investigated in the present work range from electrically small (perimeter is less than the wavelength) to electrically large (perimeter is up to ten times the wavelength). It is shown that for such an enclosure, both the RCS and SE, as functions of frequency, have sharp spikes, minima, or maxima at the resonant frequencies corresponding to the internal modes of the closed conducting sphere. Principal and higher order modes are considered. The effects of the aperture width on the perturbation of the field inside and outside of the spherical enclosure, the near field outside the cavity, the RCS and the SE are presented over a wide range of frequency. It is shown that the sharpness and amplitude of the spikes, minima, or maxima of the RCS and SE are decreased with increasing the aperture width. Also, the resonant frequencies of the enclosed spherical cavity are shifted with increasing the aperture width. For the purpose of verifying the accuracy of the obtained results for the SE of an open spherical enclosure at resonance, the obtained field configurations and distributions inside a spherical enclosure of a small aperture are compared to those of the spherical cavity modes which have already been obtained analytically. Also, some of the results concerning the RCS of a spherical enclosure are compared to other published results.

1. INTRODUCTION

A prominent problem encountered in a variety of RCS and SE in electromagnetic compatibility (EMC) studies is the prediction of the amount of energy from an electromagnetic wave that will be scattered back or penetrate through an aperture into a cavity and the level of the subsequent interaction that the coupled wave energy will have with elements within the cavity. These problems of scattering and aperture penetration have been encountered in many studies of the interactions of high power microwaves with targets such as aircraft and missiles.

On the other hand, the RCS and EMC communities must deal with the reciprocal of these shielding problems. The RCS problem concentrates on the issue of how much energy is scattered back into the far field by these cavity-backed apertures. The EMC problem associated with emission standards must deal with how much energy can escape into the far field from a device contained within a shielded enclosure or, vice-versa, how much energy, from an incident plane wave, can penetrate into a shielded enclosure through an aperture.

As a measure of the detectability of a target by radar systems, the RCS has always been an important subject of study in electromagnetics. Mathematical and computational methods to accurately predict the RCS of complex objects such as aircraft are of great interest to designers. Of particular importance is the prediction of the RCS of cavities due to its dominance to the target's overall RCS [1].

Cavity-backed apertures may be encountered in most of the air-borne or space-borne targets as air inlets and engine tubes. Such cavity-backed apertures are known to contribute a great deal to the radar cross section of jet aircrafts. Cavity-backed apertures are famous for their internal resonance which results in spikes in the scattering cross section as a function of frequency. Such spikes can easily result in recognizing the shape of a target. Consequently, such resonant spikes in the scattering cross section as a function of frequency constitute important descriptions in *target classification and identification schemes*. Thus, studying the radar cross section of targets including cavity-backed apertures over a wide range of frequency is a necessary requirement for accurate target identification.

A numerical technique is proposed in [2] for the electromagnetic characterization of scattering by a three-dimensional cavity-backed apertures. The technique combines the finite element and boundary integral method to formulate a system of equations for the solution of the aperture fields and those inside the cavity. Specifically, the finite element method is employed to formulate the fields in the cavity

region, and the boundary integral approach is used in conjunction with the equivalence principle to represent the fields in the external region.

The problem of scattering from three-dimensional cavities was treated in [3] using the Robin boundary condition iteration (RBCI) method. This hybrid method combines a differential equation for the interior and the neighborhood of the cavity and integral equation for the rest of the unbounded domain.

Another method that falls into the class of analytic-numeric or semi-analytic techniques is the method of regularization (MoR), which is described in [4]. This method solves the difficulty of error estimation encountered with the electromagnetic integral equations by analytically transforming them to well-conditioned second-kind matrix systems that have a firm basis for error estimation in Fredholm theory.

In this work, the conducting surface of the open cavity is represented by triangular-patch model and the electric field integral equation (EFIE) is applied. In spite of being not considered as a well-suited method to obtain the fields in the interior of a closed cavity, the EFIE technique is shown to be well-suited in the case of an open cavity even when the aperture is narrow.

Unlike traditional approaches, the EFIE technique used in the present work does not require the knowledge of the cavity's Green's function. For this reason, the proposed technique is applicable to arbitrary-shape cavities. However, this technique is applied, here, to treat the problem of scattering from an open spherical enclosure.

It may be worth noting that the validation of general purpose computer codes for electromagnetic problems of objects incorporating edges and cavity-backed apertures depends entirely upon comparison with the results of other proven approaches, analytical, computational or experimental. For this reason the results obtained in this work for the distributions of the internal field of the open cavity at its resonances are compared to those of the corresponding modes of the closed enclosure, which have already been given analytically [8]. It is logic that, for small aperture, the results of both cases are close to each other.

2. FORMULATION OF THE SCATTERING PROBLEM

To calculate the RCS and SE of the open spherical enclosure it is subjected to a plane wave that induces currents on the conducting surface, which, in turn, produces a scattered field. The total field (incident and scattered) satisfies the boundary condition that yields the cancellation of the tangential electric field on the spherical enclosure surface. From the knowledge of the scattered field in the far zone we

can calculate the RCS, and from the knowledge of the total field in the interior of the enclosure we can calculate the SE. The coordinate system and the angular parameters used in the present work are shown in Fig. 1.

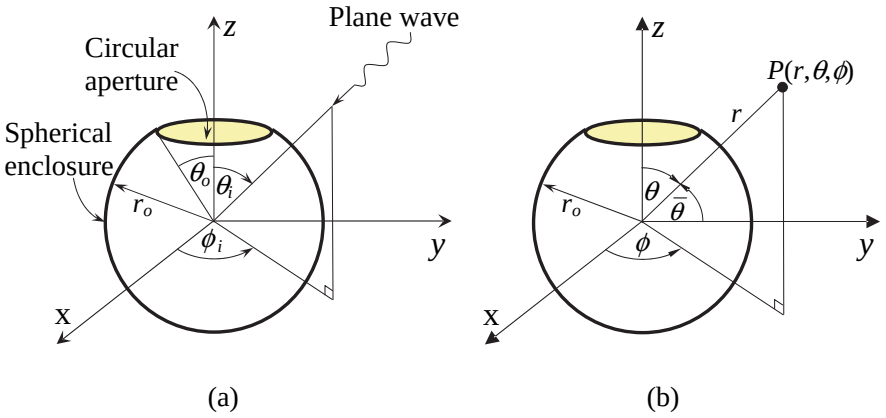

Figure 1. Conducting spherical enclosure with circular aperture subjected to a plane wave. (a) Direction of the incident wave and angular parameters. (b) Coordinate system.

2.1. Modeling the Open Spherical Enclosure

A geometrical model is required to accurately describe the spherical surface and to be suitable for the EFIE technique to be applied for treating the scattering of electromagnetic waves on the spherical enclosure.

The open spherical enclosure is a perfectly conducting surface enclosing an air region. In the present analysis, the conducting surface is composed of triangular patches as shown in Fig. 2. The more the number of triangular patches the closer the model to the actual spherical surface.

2.2. Application of the EFIE

In the present analysis, the EFIE approach described in [5–7] is used, where the induced surface current is expressed as a series summation of vector triangular basis functions with unknown amplitudes. The electric field tangential to the conducting surface is equated to zero resulting in the formation of an integral equation for the unknown current distribution on the surface of the spherical shell. The method

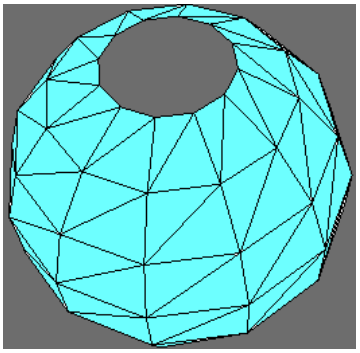

Figure 2. Triangular-patch model of the open spherical enclosure.

of moments is then applied to solve the resulting integral equation for the current on the scatterer surface. This method can briefly be outlined in the remaining of this section.

The equation solved by moment method techniques is the EFIE that results from the application of Maxwell's equations and, generally, takes the form

$$\boldsymbol{E}^{inc} = f_e(\boldsymbol{J}) \tag{1}$$

where the $\boldsymbol{E}^{inc}$ is the incident electric field and $\boldsymbol{J}$ is the induced surface current. This equation is expressed in the frequency domain; however the method of moments can also be applied in the time domain.

The first step in the moment-method solution process is to expand $\boldsymbol{J}$ as a finite sum of basis (or expansion) functions,

$$\boldsymbol{J} = \sum_{i=1}^{N} J_i \boldsymbol{b}_i \tag{2}$$

where $\boldsymbol{b}_i$ is the ith basis function and J_i is an unknown coefficient. The Rao-Wilton-Glisson (RWG) basis functions defined in [5] are the most appropriate vector basis functions for the triangular-patch model described in Section 2.1.

Next, a set of N linearly independent weighting (or testing) functions, w_i, are defined. An inner product of each weighting function is formed with both sides of the equation being solved. In the case of the EFIE (1), the inner product results in a set of N independent equations of the form,

$$\left\langle w_i, \boldsymbol{E}^{inc} \right\rangle = \langle w_i, f_e(\boldsymbol{J}) \rangle, \quad i = 1, 2, \ldots, N \tag{3}$$

By expanding $\boldsymbol{J}$ using (2), we obtain a set of N equations in N unknowns,

$$\left\langle w_i, \boldsymbol{E}^{inc} \right\rangle = \sum_{j=1}^{N} \langle w_i, f_e(J_j, \boldsymbol{b}_j) \rangle \,, \quad i = 1, 2, \ldots, N \tag{4}$$

This can be written in matrix form as,

$$[\boldsymbol{E}^{inc}] = [Z][\boldsymbol{J}] \tag{5}$$

where:

$$Z_{ij} = \langle w_i, f_e(J_j, \boldsymbol{b}_j) \rangle \tag{6}$$

The linear system of equations (5) can, now, be solved to get the unknown current distribution.

Due to the efficiency of such a technique, a small number of triangular patches may be enough to get accurate geometrical model for describing the curved surface and to get accurate results for the current and field distributions.

3. CALCULATION OF THE SCATTERED FIELD

To calculate the RCS of a scatterer, it is required to obtain the scattered field in the far zone. To calculate the SE of the open spherical enclosure, it is required to obtain the total field (incident and scattered) in the interior of the enclosure. In this section we describe a method to evaluate the scattered field in the far zone as well as in the near zone including the interior and the exterior of the spherical enclosure. By the application of the EFIE and calculating the current flowing on the scatterer surface as described above, the magnetic vector potential A and the scalar potential (can be, respectively, obtained through the following equations.

$$\boldsymbol{A}(\boldsymbol{r}) = \frac{\mu_o}{4\pi} \int\limits_S \boldsymbol{J} \frac{e^{-jk|\boldsymbol{r}-\boldsymbol{r}'|}}{|\boldsymbol{r}-\boldsymbol{r}'|} dS' \tag{7}$$

$$\Phi(\boldsymbol{r}) = \frac{1}{4\pi\varepsilon_o} \int\limits_S \sigma \frac{e^{-jk|\boldsymbol{r}-\boldsymbol{r}'|}}{|\boldsymbol{r}-\boldsymbol{r}'|} dS' \tag{8}$$

where $\boldsymbol{r}'$ is a point on the scatterer surface, $\boldsymbol{r}$ is a point in the near or far zone of free space, μ_o and ε_o are the permeability and permittivity of free space, respectively. The surface charge density σ is related to

the surface divergence of the current $\boldsymbol{J}$ flowing on the scatterer surface through the equation of continuity,

$$\nabla_s \cdot \boldsymbol{J} = -j\omega\sigma, \tag{9}$$

where $\omega = 2\pi f$; f is the frequency.

Upon the calculation of $\boldsymbol{A}$ and Φ, the scattered electric field in the near zone can be calculated using the following relation.

$$\boldsymbol{E}^{scat}(\boldsymbol{r}) = -j\omega\boldsymbol{A}(\boldsymbol{r}) - \nabla\Phi(\boldsymbol{r}) \tag{10}$$

The second term in the right hand side of (10) is evaluated by, first, discretizing the three-dimensional space and then carrying out the differentiation numerically.

Once the scattered electric field in the near zone is obtained, the scattered magnetic field can be obtained using the Maxwell curl equation,

$$\boldsymbol{H}(\boldsymbol{r}) = -\frac{1}{j\omega\mu}\nabla \times \boldsymbol{E}(\boldsymbol{r}) \tag{11}$$

The same process of discretizing the three-dimensional space and carrying out the differentiation numerically is required to evaluate the magnetic field according to (11).

4. CALCULATION OF THE RADAR CROSS SECTION OF THE SPHERICAL ENCLOSURE

RCS is the measure of the target ability to reflect radar signals in the direction of the radar receiver. RCS is defined as the ratio of the backscattered power in the direction of the radar to the power density of the wave incident at the target.

Normally, the target exists in the far zone of the radar antenna and, hence, in the calculation of the RCS a uniform plane wave is assumed incident on the target. The RCS is a function of the polarization mismatch between the wave incident on the target and that received by the radar antenna and, hence, it should be taken into consideration. In the present analysis, we assume that a linearly polarized plane wave is incident on the target. The scattered field component whose polarization is the same as that of the incident field is that used to calculate the RCS of the scatterer. Thus, the incident field at the target can be expressed as

$$\boldsymbol{E}^{inc} = \boldsymbol{a}_\xi E_o e^{-jkr} \tag{12}$$

where ξ is an arbitrary direction whose unit vector is $\boldsymbol{a}_\xi$ and r is the distance between the radar and the target.

The backscattered field at the radar antenna is a plane wave whose ξ-component can be expressed as

$$E_{\xi}^{inc} = \boldsymbol{a}_{\xi} \cdot \boldsymbol{E}^{scat} \tag{13}$$

The scattered electric field, $\boldsymbol{E}^{scat}$, in the far zone can be evaluated using (10), however, the second term in the right hand side of (10) can be neglected and, hence, the following formula is enough for calculating the scattered field in the far zone,

$$\boldsymbol{E}^{scat} = -j\omega \boldsymbol{A} \tag{14}$$

Thus, the RCS can be calculated as

$$RCS = \frac{\text{backscatter power in the direction of the radar}}{\text{power density of the incident plane wave}} = 4\pi r^2 \frac{\left|E_{\xi}^{scat}\right|^2}{|E_o|^2} \tag{15}$$

An analytic method known as "shape perturbation" method to calculate the RCS of a conducting spheroid is described in [8]. Another analytic method known as "parabolic equation" to calculate the RCS of large targets is described in [9].

In the present work, the method described in Section 3 is applied to obtain the scattered field in the far zone from which the RCS is obtained according to equation (15).

5. CALCULATION OF THE SHIELD EFFECTIVENESS OF THE SPHERICAL ENCLOSURE

The SE of the spherical enclosure can be defined as the ratio between the magnitudes of the electric field at a point in the interior of the enclosure when the enclosure is not present to the magnitude of the electric field at the same point when the enclosure is present [10]. This ratio can be calculated, in dB, as follows,

$$SE(dB) = 20 \log \frac{|E_o|}{\left|E_{\xi}^{tot}\right|} \tag{16}$$

where E_{ξ}^{tot} is the ξ-component of the total electric field, i.e., the summation of the incident and scattered fields.

6. SPHERICAL CAVITY MODES

The sharp spikes of the RCS and SE, of an open spherical enclosure, as a function of the frequency can be related to the internal resonances

of the enclosed cavity. For an open spherical enclosure of a small aperture, it is logic that the internal resonances are quite close to those of a closed spherical enclosure. Also, it is logic that the resonant frequencies of an open spherical enclosure are shifted farther from the resonant frequencies of the closed spherical enclosure with increasing the aperture width due to the reduction of the electric length of the perimeter of the enclosure. To investigate this relation, it may be worth to, first, study the resonances of the closed spherical enclosure.

Furthermore, one may claim that the solution obtained using the EFIE method may be inaccurate as the EFIE is not well-suited for analyzing the interior of conductive enclosures. This is another motivation for adding the present section. The results obtained in this work for the distribution of the internal field of the open enclosure at resonance can be realized by comparison to that of the corresponding mode of the closed enclosure, which have already been given analytically [8]. For small aperture, the results of both cases are close to each other and a comparison can be made to verify the validity of the solution.

The characteristic equation of the E-modes of the spherical cavity are given as [11]

$$j_m(u) = 0, \tag{17}$$

where $j_m(u)$ is the spherical Bessel function of first kind, $u = kr_o = 2\pi r_o/\lambda$; k is the wave-number of free space, λ is the wavelength. The integer m is the mode order that describes the angular dependence of the fields.

The resonant frequencies corresponding to the E-modes of the spherical cavity are given by the roots of (17), hence

$$f_{mn} = \frac{c}{2\pi r_o} u_{mn} \tag{18}$$

where u_{mn} is the nth root of (17). Thus, the integer n is the mode order that describes the radial dependence of the fields.

The characteristic equation of the H-modes of the spherical cavity are given as [11]

$$\frac{d}{du}[uj_m(u)] = 0 \tag{19}$$

Thus, the resonant frequencies corresponding to the H-modes of the spherical cavity are given by the roots of (19), hence

$$f'_{mn} = \frac{c}{2\pi r_o} u'_{mn} \tag{20}$$

where u'_{mn} is the nth root of (19).

To find the roots of (17) and (19), the following expressions of the spherical Bessel functions can be used [12].

$$j_0(u) = \frac{\sin u}{u} \tag{21}$$

$$j_1(u) = \frac{\sin u}{u^2} - \frac{\cos u}{u} \tag{22}$$

$$j_2(u) = \left(\frac{3}{u^3} - \frac{1}{u}\right)\sin u - \frac{2}{u^2}\cos u \tag{23}$$

The fundamental electric mode, E_{11}, has the lowest resonant frequency among all the possible modes of the spherical cavity. This mode has the following field components

$$E_r = -\frac{2r_o A}{u'_{11} r}\cos\overline{\theta} j_1\left(u'_{11}\frac{r}{r_o}\right)e^{j\omega'_{11}t} \tag{24}$$

$$E_{\overline{\theta}} = \frac{r_o A}{u'_{11} r}\sin\overline{\theta}\left[\left(u'_{11}\frac{r}{r_o}\right)j_1\left(u'_{11}\frac{r}{r_o}\right)\right]' e^{j\omega'_{11}t} \tag{25}$$

$$H_\phi = -j\sqrt{\frac{\varepsilon_r\varepsilon_o}{\mu_r\mu_o}}A\sin\overline{\theta} j_1\left(u'_{11}\frac{r}{r_o}\right)e^{j\omega'_{11}t} \tag{26}$$

with $u'_{11} = 2.745$, A is an arbitrary constant (amplitude parameter), ε_r is the relative permittivity of the material filling the spherical cavity, μ_r is the relative permeability of the material filling the spherical cavity, and $\overline{\theta}$ is the angle with the y-axis as defined in Fig. 1(b).

7. RESULTS AND DISCUSSION

This section is concerned with presenting the results showing the internal field, RCS and SE of an open spherical enclosure in the frequency ranges around the internal resonances. In all the following discussions, unless otherwise indicated, the spherical enclosure is subjected to an E_y-polarized plane wave normally incident on its aperture, i.e., $\theta_i = 0$. Also, the field distributions are plotted in the y-z section of the spherical enclosure, where the coordinate system is shown in Fig. 1(b).

7.1. Internal Field Enhancement at Internal Resonances of an Open Spherical Enclosure and the Corresponding Modes of a Closed Sphere

The wavelengths of the lowest-order resonant modes of the interior of a closed sphere can be obtained by substitution from (22) and (23) into

Table 1. Wavelengths of the spherical cavity modes in terms of the sphere radius.

Mode order		H-modes		E-modes	
m	n	u_{mn}	λ_{mn}/r_o	u'_{mn}	λ'_{mn}/r_o
1	1	4.493	1.398	2.745	2.290
2	1	5.763	1.090	3.870	1.624

(17) and (19) and then finding the roots of the resulting equations. The wavelengths of spherical cavity modes E_{11}, E_{21}, H_{11} and H_{21} are given in table (1) in terms of the sphere radius.

Fig. 3(a) shows the electric field distribution for the spherical cavity mode E_{11} in the r-$\overline{\theta}$ plane defined by: $\phi = 90°$. This distribution is given by the expressions (24) and (25). It should be noted that the origin is at the center of the sphere and the coordinate system is that defined in Fig. 1(b). It is clear in Fig. 3(a) that E_r is even and $E_{\overline{\theta}}$ is odd about y-axis ($\overline{\theta} = 0$).

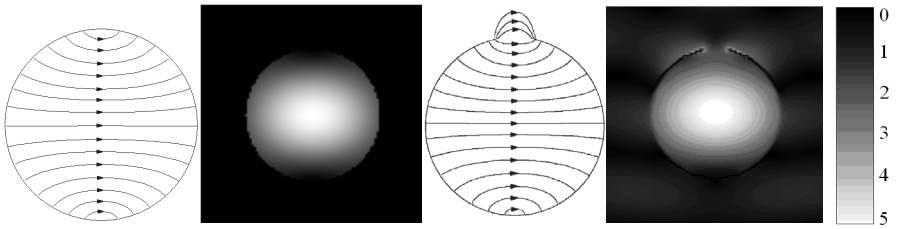

(a) (b)

Figure 3. Distribution of the total electric field, $f = 0.4367\,\text{GHz}$, (a) E_{11} of a closed sphere. (b) Near field of an open spherical enclosure of $\theta_o = 10°$ subjected an E_y-polarized plane wave normally incident on the aperture.

Fig. 3(b) shows the electric field distribution inside and around a conducting spherical enclosure with circular aperture of $\theta_o = 10°$ subjected to an E_y-polarized plane wave normally incident on the aperture of the enclosure, i.e., $\theta_i = 0$. The operating frequency is $0.4367\,\text{GHz}$, which is the resonant frequency corresponding to the E_{11} internal mode of the spherical enclosure whose distribution is shown in Fig. 3(a). By comparing Figures 3(a) and 3(b), the field pattern

of the E_{11} spherical cavity mode can easily be recognized inside the open spherical enclosure. Thus, in the case of small aperture, the E_{11} mode is excited inside the spherical enclosure when the frequency of the incident plane wave is close to the resonant frequency of this mode.

Fig. 4(a) shows the electric field distribution for the spherical cavity mode E_{21} in the r-$\overline{\theta}$ plane defined as: $\phi = 90°$. This distribution can be obtained from [11]. Fig. 4(b) shows the electric field distribution inside and around a conducting spherical enclosure with circular aperture of $\theta_o = 10°$ subjected to an E_y-polarized plane wave normally incident on the aperture of the enclosure, i.e., $\theta_i = 0$. The operating frequency is 0.6155 GHz, which is the resonant frequency corresponding to the E_{21} internal mode of the spherical enclosure whose distribution is shown in Fig. 4(a). By comparing Figures 4(a) and 4(b), it becomes clear that, in the case of small aperture, the E_{21} mode is excited inside the spherical enclosure when the frequency of the incident plane wave is close to the resonant frequency of this mode.

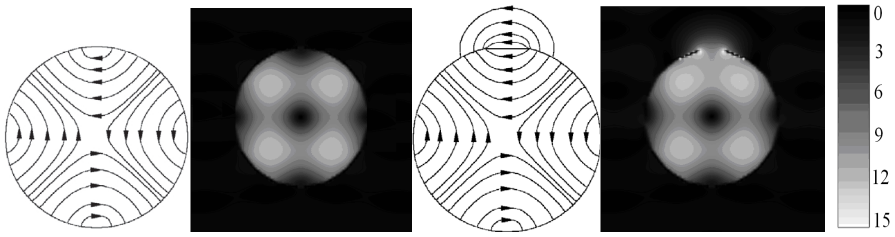

Figure 4. Distribution of the total electric field, $f = 0.6155$ GHz, (a) E_{21} of a closed sphere. (b) Near field of an open spherical enclosure of $\theta_o = 10°$ subjected an E_y-polarized plane wave normally incident on the aperture.

In the two cases discussed above, the electric field intensity in the interior of the enclosure is much higher than that in the exterior of the enclosure. Accordingly, one can deduce that, at the frequencies corresponding to the internal resonances of the spherical enclosure, most of the power of the incident wave is sucked into the interior of the open enclosure. This can considerably affect the RCS and the SE of such an enclosure at the resonant frequencies.

7.2. Radar Cross Section of a Conducting Sphere

For the sake of investigating the capability of the applied technique to accurately calculate the RCS of a conducting target that encloses a

cavity, and to provide a reference to compare with when obtaining the RCS of an open spherical enclosure, the method described in Section 4 is applied to calculate the RCS of a closed sphere. The RCS of such a closed enclosure is obtained over a wide range of frequency as shown in Fig. 5. The results are compared with those of [8], which are obtained analytically using the shape perturbation method. The comparison shows good agreement, which ensures the validity of the applied technique and the accuracy of the obtained results.

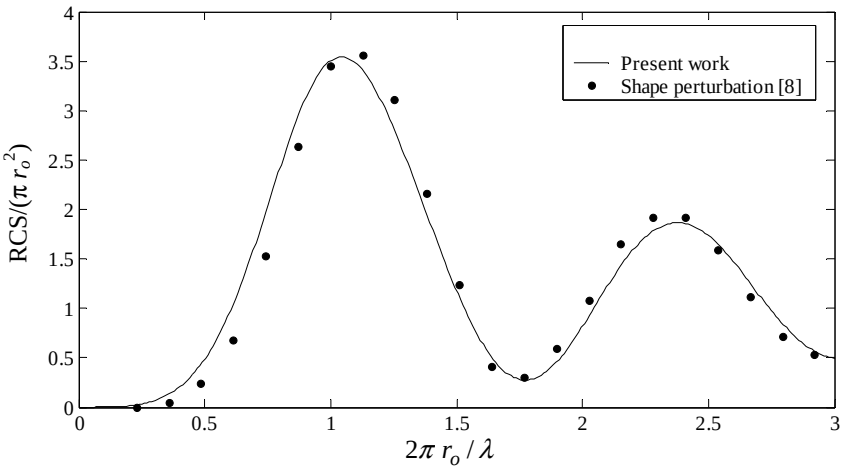

Figure 5. Radar cross section of a conducting sphere compared with the results of [8].

7.3. Radar Cross Section of Open Spherical Enclosure at Internal Resonances

Fig. 6 shows a comparison between the RCS of a conducting sphere and that of an open spherical enclosure with $\theta_o = 10°$. Both targets have radii of 30 cm and are subjected to a plane wave incident with $\theta_i = 0$. Thus, the plane wave is normally incident on the aperture of the spherical enclosure. The RCS is calculated over a very wide band of frequency ranging from 0 to 1.6 GHz, i.e., from $(2\pi r_o)/\lambda = 0$ to $(2\pi r_o)/\lambda = 10$. The EFIE technique described in [13] is applied to get the RCS of both targets, where the spherical surface is constructed up using 2061 triangular patches. As shown in Fig. 6, the normalized RCS of the closed sphere, oscillates around the unity with varying the frequency where the first peak (over shoot) occurs at $(2\pi r_o)/\lambda = 1$. The amplitude of oscillations diminishes and the normalized RCS

asymptotically approaches the unity with increasing the frequency. This is a well known behavior of the RCS of a conducting sphere, which has already been obtained analytically. The agreement of the results obtained in the present work with such well known behavior ensures the validity and accuracy of the employed technique to get the RCS of targets of different sizes ranging from electrically small to electrically large.

For the frequencies below 0.35 GHz or, equivalently, for $(2\pi r_o)/\lambda < 2.2$, the normalized RCS of the open enclosure is almost the same as that of the closed one. For the higher frequencies, the RCS of the open spherical enclosure is significantly different from that of the closed one and has sharp spikes at the frequencies corresponding to the internal resonances as shown in Fig. 6. A spike is a sharp minimum immediately followed by a sharp maximum or a sharp maximum immediately followed by a sharp minimum. These spikes play an important role in recognizing the shape of such a target in target identification schemes. It is shown in the figure that, apart from very narrow bands around the resonant frequencies, the aperture has the effect of globally increasing the RCS of the spherical enclosure in comparison with that of the closed one over the entire frequency range.

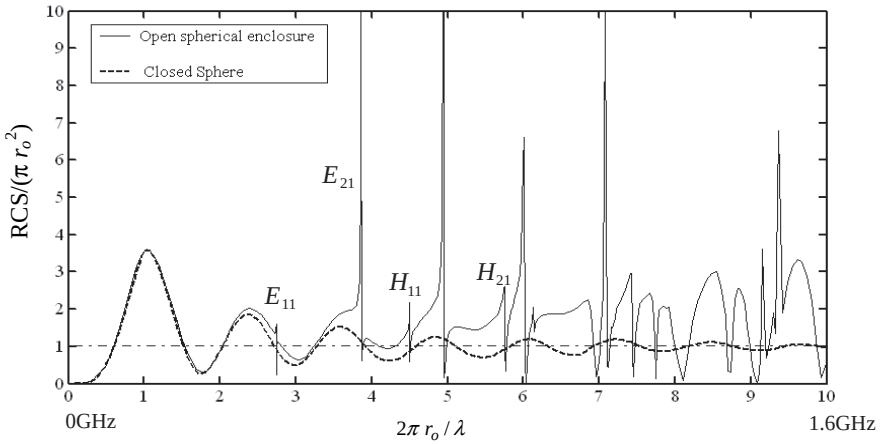

Figure 6. RCS of a conducting sphere and an open spherical enclosure against the frequency, $r_o = 30\,\text{cm}$, $\theta_o = 10^\circ$, $\theta_i = 0$.

Figures 7 and 8 show comparisons among the RCS of a spherical enclosure in three cases: (i) the plane wave is normally incident on the aperture of an open enclosure, (ii) the plane wave is incident on the back of the aperture of the same enclosure, and (iii) the plane wave

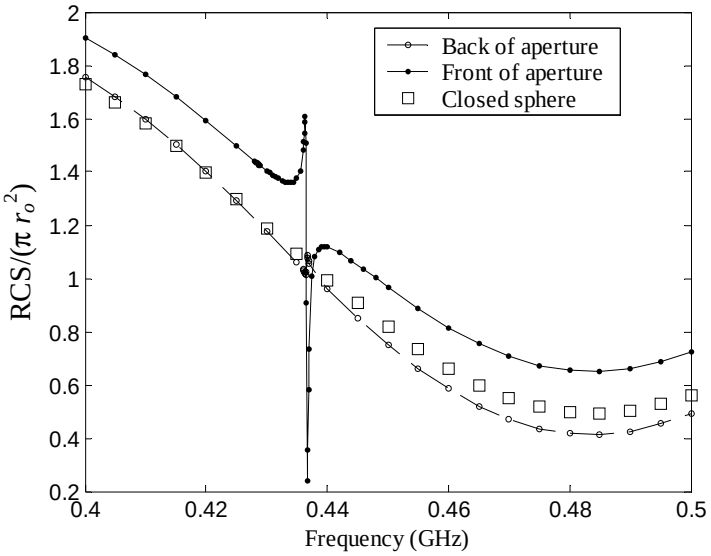

Figure 7. A spike of the RCS of the open spherical enclosure at the resonance corresponding to the E_{11} mode of the spherical cavity, $r_o = 30\,\text{cm}$, $\theta_o = 10^\circ$.

is incident on a closed enclosure of the same radius. Fig. 7 presents the three cases in the frequency range around the internal resonance corresponding to the E_{11} mode, whereas Fig. 8 presents the same cases in the frequency range around the internal resonance corresponding to the E_{21} mode. As shown in both figures, the RCS in the case of a plane wave incident on the back of the aperture ($\theta_i = 180^\circ$) is very close to that of a closed sphere with a very weak spike at resonances, whereas the RCS in the case of a plane wave incident normally on the aperture is significantly higher than that of a closed sphere over the entire frequency range with a strong spike at resonance.

7.4. Shield Effectiveness of Open Spherical Enclosure at Internal Resonances

The SE effectiveness of the open spherical enclosure can be calculated as described in Section 5, where the field inside the enclosure is obtained by applying the method described in [14]. As shown in Fig. 9, the SE of an open spherical enclosure of small aperture, has a sharp minimum within a very narrow frequency interval around the resonant frequency corresponding to the mode of the spherical cavity. The worst

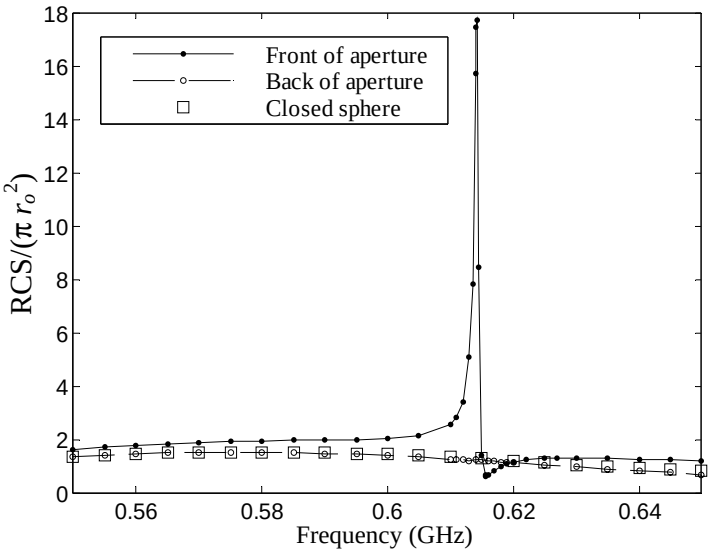

Figure 8. A spike of the RCS of the open spherical enclosure at the resonance corresponding to the E_{21} mode of the spherical cavity, $r_o = 30\,\text{cm}$, $\theta_o = 10^\circ$.

case of the SE of an open spherical enclosure occurs when the plane wave is normally incident on its aperture, i.e., $\theta_i = 0$. When the plane wave is incident on the back of the aperture, i.e., when $\theta_i = 180^\circ$, the SE is better by about 8–12 dB, however, a sharp minimum is still occurring at resonance.

At the resonance corresponding to the E_{21} mode of the spherical cavity, the situation is some how different than that at the E_{11} resonance. At the E_{21} resonance, and as shown in Fig. 10, the SE has a sharp spike (a sharp minimum immediately followed by a sharp maximum). In the case when $\theta_i = 0$, the spike occurring in the SE at resonance is much greater than that occurring when as shown in Fig. 10.

The sharp decrease of the SE of such open enclosure at the internal resonances can be attributed to the internal field enhancement occurring at the resonant frequency due to the formation of the E_{21} resonant mode as discussed before in Section 7.1. Fig. 11 shows the sudden enhancement of the internal field as the frequency changes from 0.6142 GHz (anti-peak) to 0.6190 GHz (peak) where the SE dramatically changes from 2 dB to 46 dB.

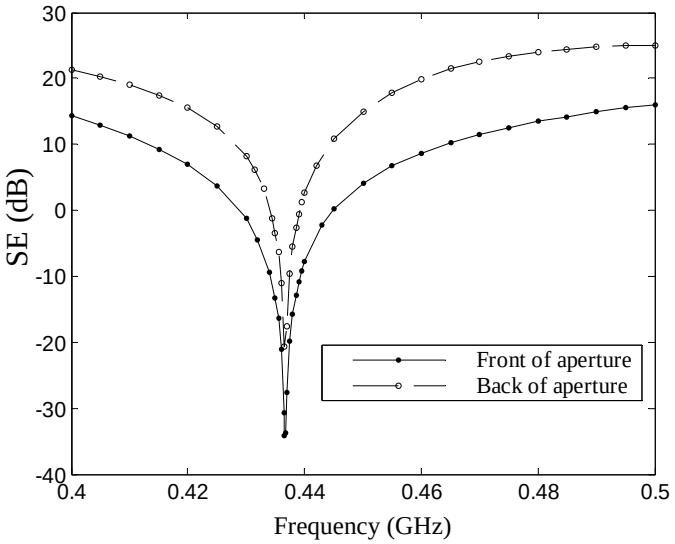

Figure 9. The shield effectiveness of an open spherical enclosure in the frequency range around the resonant frequency corresponding to the E_{11} spherical cavity mode, $r_o = 30\,\text{cm}$, $\theta_o = 10^\circ$.

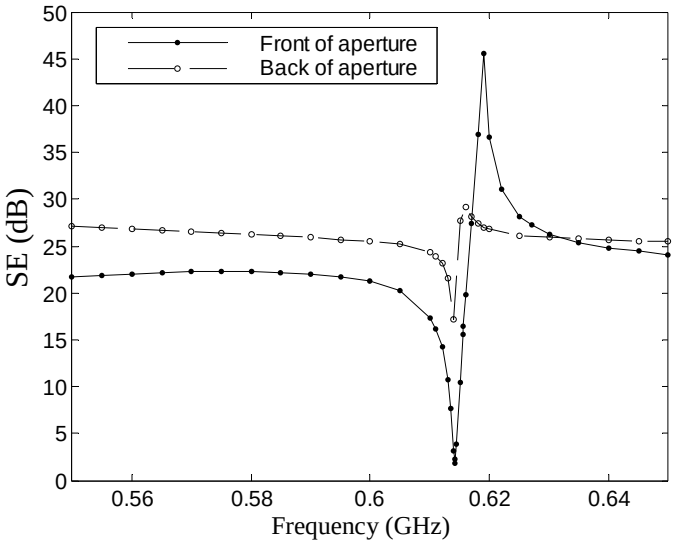

Figure 10. The shield effectiveness of an open spherical enclosure in the frequency range around the resonant frequency corresponding to the E_{21} spherical cavity mode, $r_o = 30\,\text{cm}$, $\theta_o = 10^\circ$.

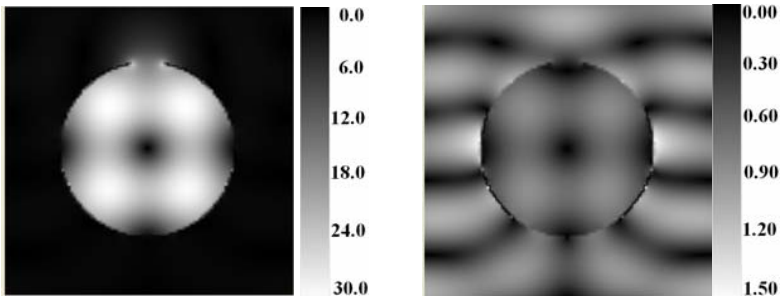

(a) (b)

Figure 11. Distribution of the near field of an open spherical enclosure of $r_o = 30\,\text{cm}$, $\theta_o = 10^\circ$ subjected an E_y-polarized plane wave normally incident on the aperture at the spike corresponding to the E_{21} resonant mode. (a) SE anti-peak: $f = 0.6142\,\text{GHz}$. (b) SE peak: $f = 0.6190\,\text{GHz}$.

7.5. Dependence of Internal Field and SE of Open Spherical Enclosure on the Aperture Width

So far, we have studied the case of a spherical enclosure with narrow aperture. To investigate the effect of the aperture width on the internal field of the enclosure, we plot the electric field intensity at the centre of the spherical enclosure against the frequency with varying the aperture width from $\theta_o = 10^\circ$ to $\theta_o = 30^\circ$ due to an E_y-polarized plane wave that is normally incident on the aperture. This is presented in Fig. 12, where the selected range of frequency is around the resonance corresponding to the E_{11} mode. As shown in this figure, for very small aperture, the internal field shows very sharp peak of high amplitude at the resonance, but however, as the aperture width increases, the peak becomes less sharp and of lower amplitude. Also, its shown that the resonant frequency is decreased with increasing the aperture width. The smaller the aperture is, the closer the resonant frequency to that of the mode of the closed sphere.

Fig. 13 shows the electric field distribution inside and around the open enclosure at the resonance corresponding to the E_{11} mode due to an E_y-polarized plane wave that is normally incident on the aperture with varying the aperture width from $\theta_o = 10^\circ$ to $\theta_o = 30^\circ$. For narrow-aperture enclosure, the field is mainly concentrated inside the enclosure and is almost identical to that of the E_{11} mode of the closed sphere with negligible perturbation due to the aperture as discussed in Section 7.2. As the aperture width increases, the intensity of the field is decreased inside the enclosure and is relatively increased in the region

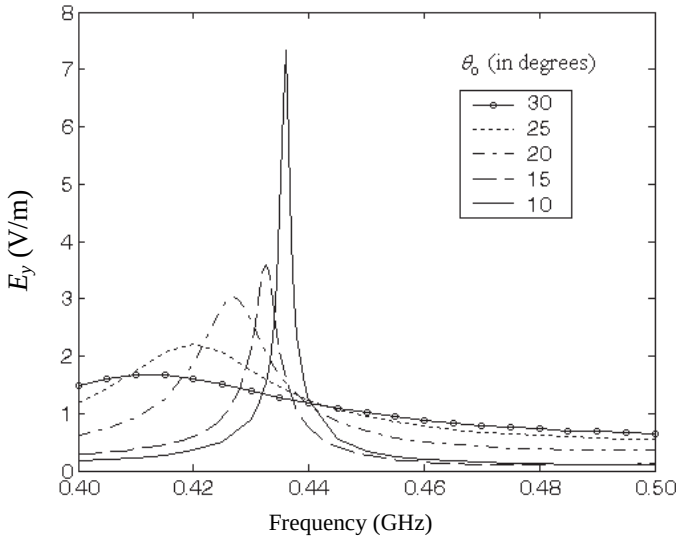

Figure 12. Variation of the electric field at the center of the spherical enclosure for different values of the aperture width in a range of frequency around the E_{11} resonance, $r_o = 30\,\text{cm}$.

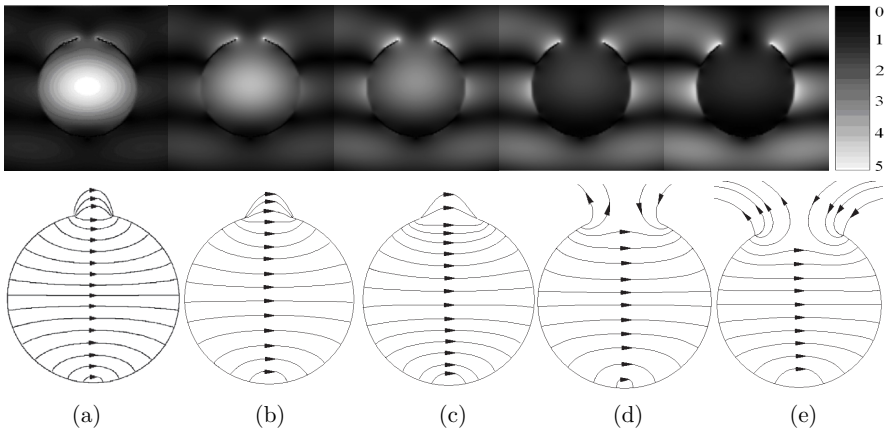

Figure 13. Distribution of the electric inside and around the spherical enclosure due an incident plane wave at the resonance corresponding to the mode for different values of the aperture width $r_o = 30\,\text{cm}$. (a) $f = 0.4360\,\text{GHz}$, $\theta_o = 10°$. (b) $f = 0.4325\,\text{GHz}$, $\theta_o = 15°$. (c) $f = 0.4275\,\text{GHz}$, $\theta_o = 20°$. (d) $f = 0.4200\,\text{GHz}$, $\theta_o = 25°$. (e) $f = 0.4150\,\text{GHz}$, $\theta_o = 30°$.

outside the enclosure. For a wide aperture, the field distribution of the E_{11} mode is still recognized in the interior of the spherical enclosure but, however, is significantly perturbed by the wide aperture.

To investigate the effect of the aperture width on the SE of the enclosure, Fig. 14 shows a plot for the SE of the spherical enclosure against the frequency with varying the aperture width from $\theta_o = 10^\circ$ to $\theta_o = 30^\circ$. An E_y-polarized plane wave is assumed to be normally incident on the aperture. The selected range of frequency is around the resonance corresponding to the mode. As shown in this figure, for very small aperture, the SE shows very sharp minimum of high amplitude at the resonance, but however, as the aperture width increases, the minimum of the SE is less sharp, has lower amplitude and occurs at a lower frequency.

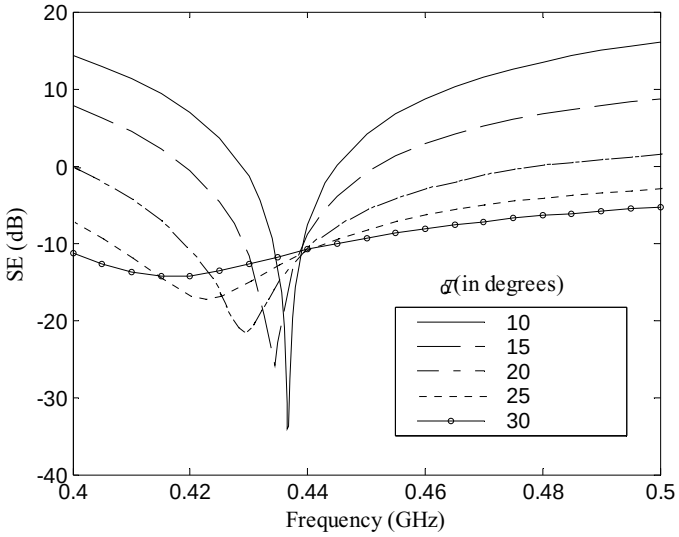

Figure 14. The shield effectiveness of an open spherical enclosure in a range of frequency around the resonant frequency corresponding to the E_{11} spherical cavity mode for different values of the aperture width, $r_o = 30\,\text{cm}$.

8. CONCLUSION

It is shown that both the RCS and SE of an open spherical enclosure, as functions of frequency, have sharp spikes, maxima, or minima at the resonant frequencies corresponding to the internal modes of the closed conducting sphere. The sharpness and amplitude of the spikes of the RCS and SE at internal resonances are decreased with increasing the aperture width. Also, it is found that the resonant frequency corresponding to the E_{11} mode is shifted with increasing the aperture width. The sharp reduction or enhancement of the SE of the open spherical enclosure at internal resonances is attributed to the internal field enhancement or diminishing, respectively, at resonance where the distribution of internal field intensity is investigated and presented at the peaks and anti-peaks of the SE as a function of the frequency. The accuracy of the obtained results for the SE of an open spherical enclosure at resonance is verified by comparing the obtained field configurations and distributions inside a spherical enclosure of a small aperture to those of the spherical cavity modes which have already been obtained analytically. Also, the obtained solutions for the RCS of a spherical enclosure are compared to other published results showing good agreement, which ensures the capability of the employed technique to deal with conducting objects with cavities and cavity-backed apertures.

REFERENCES

1. Ammari, H., G. Bao, and A. W. Woods, "A cavity problem for Maxwell's equations," *Methods and Applications of Analysis*, Vol. 9, No. 2, 249–260, June 2002.
2. Jin, J. M. and J. L. Volakis, "A finite element-boundary integral formulation for scattering by three-dimensional cavity-backed apertures," *IEEE Trans. Antennas and Prop.*, Vol. AP-39, 97–104, Jan. 1991.
3. Alfonzetti, S., B. Azzerboni, and G. Borzi, "Scattering from three-dimensional cavity-backed apertures in infinite ground plane by RBCI," *IEEE Trans. Magnetics*, Vol. 36, 917–920, Jul. 2000.
4. Vinogradov, S. S., P. D. Smith, and E. D. Vinogradova, *Canonical Problems in Scattering and Potential Theory*, Part I: Canonical structures in potential theory, Part II: Acoustic and electromagnetic diffraction by canonical structures, Chapman & Hall/CRC Press, 2002.
5. Rao, S. M., D. R. Wilton, and A. W. Glisson, "Electromagnetic

scattering by surfaces of arbitrary shape," *IEEE Trans. Antennas Propagat.*, Vol. 30, 409–418, May 1982.

6. Yla-Oijala, P., M. Taskinen, and J. Sarvas, "Surface integral equation method for general composite material and dielectric structures with junctions," *Progress In Electromagnetics Research*, PIER 52, 81–108, 2005.
7. Hanninen, I., M. Taskinen, and J. Sarvas, "Singularity subtraction integral formulae for surface integral equations with RWG, rooftop and hybrid basis functions," *Progress In Electromagnetics Research*, PIER 63, 243–278, 2006.
8. Kotsis, A. D. and J. A. Roumeliotis, "Electromagnetic scattering by a metallic spheroid using shape perturbation method," *Progress In Electromagnetics Research*, PIER 67, 113–134, 2007.
9. Mallahzadeh, A. R. and M. Soleimani, "RCS computation of airplane using parabolic equation," *Progress In Electromagnetics Research*, PIER 57, 265–276, 2006.
10. Khan, Z. A., C. F. Bunting, and M. D. Deshpande, "Shielding effectiveness of metallic enclosures at oblique and arbitrary polarizations," *IEEE Trans. Elctromagn. Compat.*, Vol. 47, No. 1, Feb. 2005.
11. Starton, J. A., *Electromagnetics Theory*, Section 9.24, McGraw-Hill, New York and London, 1941.
12. Abramowitz, M. and I. Segun, *Handbook of Mathematical Functions with Formulas, Graphs, and Mathematical Tables*, Chapter 10, Dover Publication Inc., New York, 1965.
13. Hussein, K. F. A., "Fast computational algorithm for EFIE applied to arbitrarily-shaped conducting surfaces," *Progress In Electromagnetics Research*, PIER 68, 339–357, 2007.
14. Hussein, K. F. A., "Efficient near-field computation for radiation and scattering from conducting surfaces of arbitrary shape," *Progress In Electromagnetics Research*, PIER 69, 267–285, 2007.